Journal of the European Ceramic Society **15** (1995) 25–32

0955-2219/95/$9.50

Grain Boundary Ionic Conduction in Zirconia-based Solid Electrolyte with Alumina Addition*

Xin Guo,[a]‡ Chao-Qun Tang[b] & Run-Zhang Yuan[a]

[a] State Key Laboratory for Synthesis and Processing of Advanced Materials, Wuhan University of Technology, Wuhan, Hubei Province 430070, People's Republic of China
[b] Department of Physics, Huazhong University of Science and Technology, Wuhan, Hubei Province 430074, People's Republic of China

(Received 2 February 1994; accepted 1 April 1994)

Abstract

The grain boundary resistance of 9 mol% Y_2O_3-stabilized ZrO_2 with Al_2O_3 addition was measured by the complex impedance approach. The effect of Al_2O_3 addition on the grain boundary resistance was analyzed from the aspects of microstructure and crystal defects by means of SEM, EPMA, TEM and the positron annihilation technique. The Al_2O_3 addition up to 5 mol% was found to reduce the grain boundary resistance per unit surface area of the grain boundaries and the activation energy for the grain boundary resistance. This phenomenon was explained by the scavenging of the grain boundary impurities, e.g. SiO_2, by the Al_2O_3 and the formation of the crystal grain boundary phases with very high defect concentration. By the analyses with a simplified theoretical model, the Al_2O_3 addition was considered to have no detrimental effect on the emf of the ZrO_2 oxygen sensor.

1 Introduction

In polycrystal ceramic materials, grain boundaries have a large, often controlling importance for properties. The studies on grain boundary behavior are essential for the design of ceramic materials, and the control and optimization of their performances. Thus a concept of 'grain boundary engineering' was put forward, i.e. to improve the properties of ceramics by modifying grain boundaries.[1] Now the grain boundaries of ZrO_2-based solid electrolyte have attracted much attention.

As one of the most important solid electrolytes, much research has been performed on ZrO_2. Although the research results are not totally in keeping with each other, the following points have been clarified: (1) the grain resistivity of polycrystal ZrO_2 is equivalent to that of a single crystal, and it is usually not affected by sintering temperature, atmosphere and heat treatment;[2] (2) the efforts to reduce the grain resistivity by changing composition (e.g. adding Y_2O_3, CaO, MgO, rare earth oxides, and two, three or more oxides are simultaneously added) are now nearly exhausted, the optimum stabilizer concentrations, e.g. 8–9 mol% Y_2O_3 or 13–14 mol% CaO have been generally established;[3] it is difficult to find a new stabilizer which can remarkably reduce the grain resistivity in a expectable period; (3) the property and structure of grain boundary phases are strikingly influenced by impurity, sintering temperature, atmosphere and heat treatments;[4] (4) the ZrO_2 grain boundary resistivity may be lower or higher than that of grain due to the difference of segregated elements and variation of grain boundary structure.[5,6] All these points suggest that a feasible way to further enhance the ionic conduction of ZrO_2 is to reduce the grain boundary resistivity by adding a new kind of ingredient. In order to densify ZrO_2 during sintering, certain amounts of Al_2O_3 were often added to ZrO_2.[7] After further study, it was discovered that Al_2O_3 can also reduce the resistance of ZrO_2.[8] In this paper, Al_2O_3 up to 5 mol% is added and the grain boundary resistance is studied.

2 Experimental Procedure

2.1 Preparation of specimens

The compositions of specimens are listed in Table 1. Powders used to produce the specimens were prepared from $ZrOCl_2 \cdot 8H_2O$, YCl_3 and $AlCl_3$ by

* Project supported by China Postdoctoral Science Foundation.
‡ To whom correspondence should be addressed.

Table 1. Compositions of specimens

Specimen	*Composition*
0AYZ	ZrO_2–9 mol% Y_2O_3
1·5AYZ	ZrO_2–9 mol%Y_2O_3–1·5 mol% Al_2O_3
5AYZ	ZrO_2–9 mol% Y_2O_3–5 mol% Al_2O_3

a coprecipitation method, average particle sizes measured by a centrifugal particle size analyzer (type SA-CP3) are 0·45 μm, 0·40 μm and 0·48 μm respectively. The powders were subsequently pressed into pellets (22 mm in diameter by 4 mm thick) at 200 MPa, then sintered at 1600°C for 2 h. The platinum electrodes were applied to the ZrO_2 specimens by the decomposition of chloroplatinic acid at 1000°C.

2.2 Measurements and analyses

The specimens under went the following measurements and analyses. (1) Resistances were measured by the complex impedance approach in a frequency range of 20 Hz to 1 MHz with a HP4285A precision LCR meter, the grain and grain boundary resistances were separated out by the analyses of the complex plots. (2) Al distribution information inside the specimens was examined by EPMA (type JCXA-733) on the specimens polished and coated with carbon. (3) Microstructure studies were carried out with SEM (type JSM-35C) and TEM (type H-800, Philips-CM_{12}/STEM). (4) Crystal defect changes were detected by the positron annihilation technique (CANBERRA Series 35).

3 Results

3.1 Grain boundary resistance

The complex impedance approach has been used extensively in the examination and development of solid electrolytes after the initial report by Bauerle.[9] This approach can effectively probe the grain resistance as well as the resistance across grain boundaries and electrode/electrolyte interfaces.

The grain boundary resistances R_{gb} of the specimens were measured at 440°C and 500°C; the results are listed in Table 2. In order to explain further the measured results, the grain boundary resistances per unit surface area of grain boundaries R_{gbs} were calculated from[10]

$$R_{gbs} = \rho_{gb}/D = R_{gb}(S/l)/D \qquad (1)$$

where ρ_{gb} is the grain boundary resistivity, S/l is the cross-section/length ratio of the specimen and D the grain boundary density. R_{gbs} has been used before by Miyayama and coworkers to explain intrinsic and extrinsic grain boundary phenomena,[8,10] because R_{gbs} values contain no microstructural effects. The R_{gbs} values are also listed in Table 2. For the case studied in this paper, if space charges resulting from the irregularity of lattice can account for the resistance of the grain boundary surface (intrinsic effect), the R_{gbs} should be constant, i.e. independent of Al_2O_3 content. However, for the extrinsic effects (impurity dominated), when the Al_2O_3 addition increases, the concentration of Al_2O_3 per unit surface area of grain boundaries also increases, notwithstanding the change of the grain boundary density D. Therefore, the R_{gbs} should be affected by the Al_2O_3 addition; this, in fact, is the case for the specimens used in this study. The R_{gbs} of the specimen 0AYZ is much higher than those of the specimens 1.5AYZ and 5AYZ; the specimen 5AYZ has the smallest R_{gbs} value.

Activation energies for the grain boundary resistance can be calculated from the Arrhenius equation

$$R = A \exp(E/KT) \qquad (2)$$

where K and T have their usual meanings. The values are listed in Table 2. The specimen 0AYZ has the largest grain boundary resistance activation energy E_{gb}, and E_{gb} decreases with increasing Al_2O_3 content.

3.2 Positron annihilation

The measurements of positron lifetime spectra were carried out at room temperature (21 ± 1)°C by a fast–fast coincidence lifetime spectrometer with a resolution of 230ps. A ^{22}NaCl positron source was used in the measurements. A normal specimen–source–specimen sandwich arrangement was adopted. A total of 10^6 counts in each spectrum were collected. After substracting the source and background contribution, all lifetime spectra were

Table 2. The grain boundary resistances and the activation energy of the specimens

Specimen	*Measured at 440°C*		*Measured at 500°C*		*Activation energy*
	R_{gb} (Ω)	R_{gbs} (Ω/cm²)	R_{gb} (Ω)	R_{gbs} (Ω/cm²)	E_{gb}(kJ/mol)
0AYZ	1 400	6·5	300	1·4	117·6
1·5AYZ	215	4·1	50	0·96	111·3
5AYZ	175	1·2	50	0·35	95·6

Table 3. Positron lifetime parameters

Specimen	τ_1 *(ps)*	τ_2 *(ps)*	τ_3 *(ps)*	I_1 *(%)*	I_2 *(%)*	I_3 *(%)*	$K(\mu s^{-1})$
0AYZ	239	269	1 802	90·5	8·2	1·3	38·3
1·5AYZ	205	353	1 685	90·5	7·6	1·5	155·4
5AYZ	204	375	1 806	92·0	6·9	1·2	153·7

analyzed with three components by the program POSITRONFIT EXTENDED. Lifetimes τ_1, τ_2 and τ_3 and their relative intensities I_1, I_2 and I_3 were obtained (listed in Table 3). The long lifetime component τ_3, whose intensity is about 1·4%, may arise from the positron annihilation in the positron source and associated foils, and/or interfaces that are unavoidable with the sandwich arrangement, so τ_3 will not be discussed. The short lifetime component τ_1 reflects the positron annihilation feature in perfect lattices, and τ_2 is the positron lifetime in crystal defects. According to the two-state trapping model,[11] the trapping rate of the defects to positron K can be derived,

$$K = I_2 \Big/ \left(\frac{1}{\tau_1} - \frac{1}{\tau_2}\right) \tag{3}$$

The K values are listed in Table 3. Because $K = \mu C$, where C is the concentration of defects and μ is the specific trapping rate which can be considered as a constant when the type or structure of the defects does not change; thus the change of K can roughly reflect the change of the defect concentration. The K value increases when Al_2O_3 is added to ZrO_2, this tendency is opposite to that of the grain boundary resistance per unit surface area of grain boundaries R_{gbs}; in other words, with increasing Al_2O_3 content, the defect concentration of the specimens increases, and consequently the R_{gbs} value decreases.

3.3 Microstructure

The solubility of Al_2O_3 in ZrO_2 grain is very low, only 0·5 mol% Al_2O_3 can be dissolved in Y_2O_3-stabilized ZrO_2 sintered at 1700°C and cooled at 220°C/h,[8] and the solubility of Al_2O_3 is about 0·1 mol% when sintered at 1300°C.[12] So it is obvious that the Al_2O_3 additions in the present work are far beyond the Al_2O_3 solubility.

Figure 1 shows the scanning electron micro-

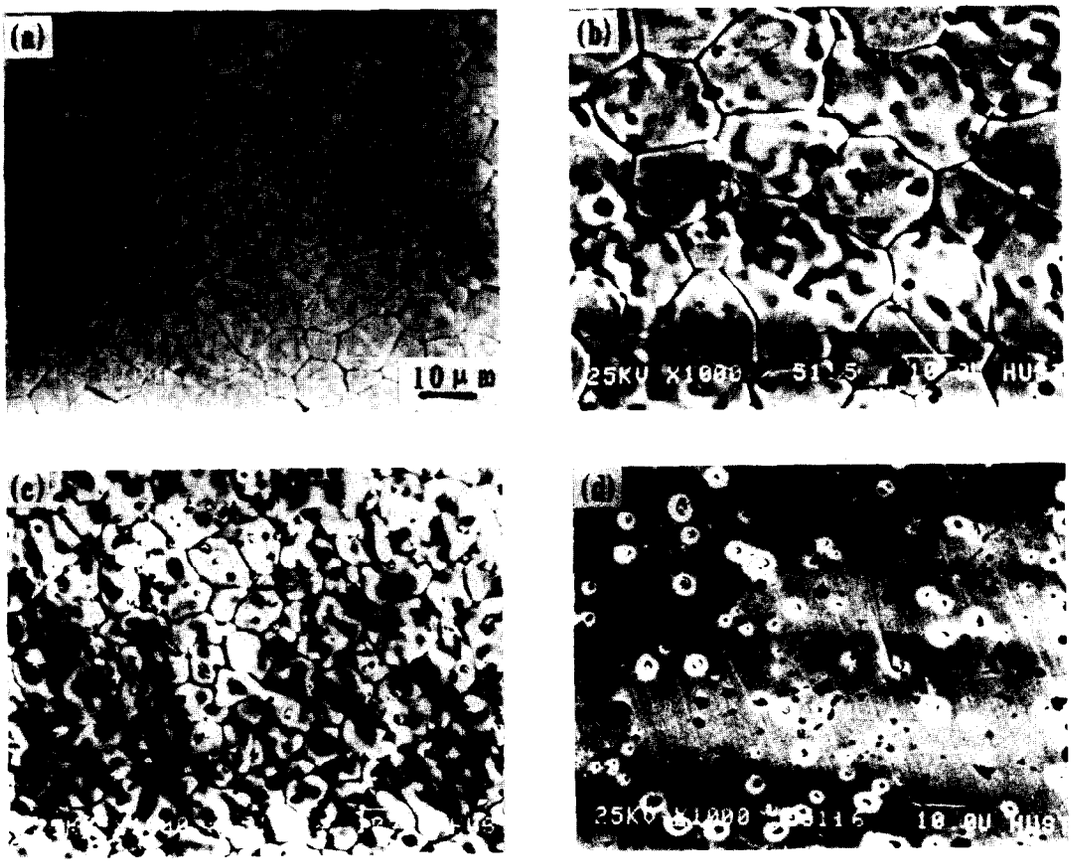

Fig. 1. Scanning electron micrographs of the surfaces of as-sintered specimens. (a) 0AYZ, (b) 1·5AYZ, (c) 5AYZ, (d) 1·5AYZ, polished surface.

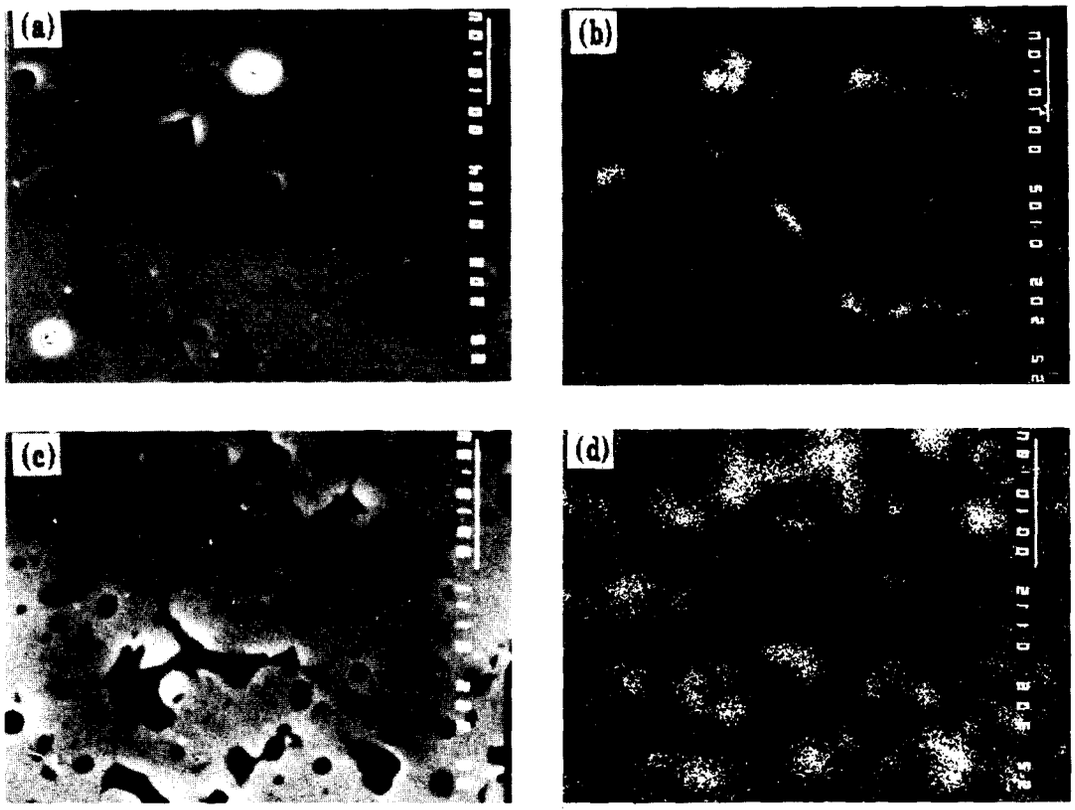

Fig. 2. EPMA photographs of the specimens with different Al_2O_3 content. (a), (b) 1·5AYZ, (c), (d) 5AYZ.

graphs of the surfaces of the as-sintered specimens 0AYZ, 1·5AYZ and 5AYZ, and the polished surface of the specimen 1·5AYZ. The specimen 0AYZ has a homogeneous mono-phase structure, while Al_2O_3 particles can be observed as bright or dark spots in the specimens 1·5AYZ and 5AYZ; the Al_2O_3 particles are situated both inter- and intragranularly. Because there are quite large differences in the elastic modulus and the thermal expansion coefficient between Al_2O_3 and ZrO_2, the intragranular Al_2O_3 particles are always accompanied by pores, which can be seen from the polished surface.

Figure 2 shows the EPMA analysis results, in which photographs (a) and (c) are scattered electron images and photographs (b) and (d) display the Al distributions. From these photographs, it can be seen that Al is mainly segregated at grain boundaries, and that the Al segregation is more serious in the specimen 5AYZ. Some small dark spots inside grains shown in the scattered electron images are Al_2O_3 particles and pores. Apparent enrichment of Si and Ca at grain boundaries was not observed.

Because of the segregation of Al_2O_3 and impurities at grain boundaries, grain boundary phases are often formed. Two types of grain boundary phases were discovered in the specimens with Al_2O_3 addition; one type is shown in Fig. 3. The small bright particle situated at the triple point of ZrO_2 grains is an Al_2O_3 particle (Fig. 3(a)), the grain boundary phases have a peculiar morphology. Figure 3(b) is the SADP of the grain boundary phases, the diffraction rings indicate that the grain boundary phases consist of large amount of crystallites. The ratio of the square radii of the diffraction rings is

$$R_1^2 : R_2^2 : R_3^2 : R_4^2 : R_5^2 : R_6^2 \approx 1 : 2 : 3 : 6 : 7 : 9 \quad (4)$$

According to the ratio and brightness distribution of the diffraction rings, these crystallites do not have crystal structure of α-Al_2O_3 or cubic ZrO_2; because of the large errors usually involved in electron diffractions, it is still difficult to determine the crystal structure of the crystallites. The composition of the grain boundary phases measured by EDAX is given in Table 4. An enrichment of Al was found and no impurities such as Si, Ca were detected. However, for the crystal grain boundary phases at different regions of the specimen, different SADP patterns are produced and different Al, Y and Zr concentrations are measured by EDAX. The phases may be con-

Table 4. Composition of the crystal grain boundary phases measured by EDAX

Element	*wt%*	*at.%*
Al	2·62	8·29
Y	15·76	15·17
Zr	81·62	76·54

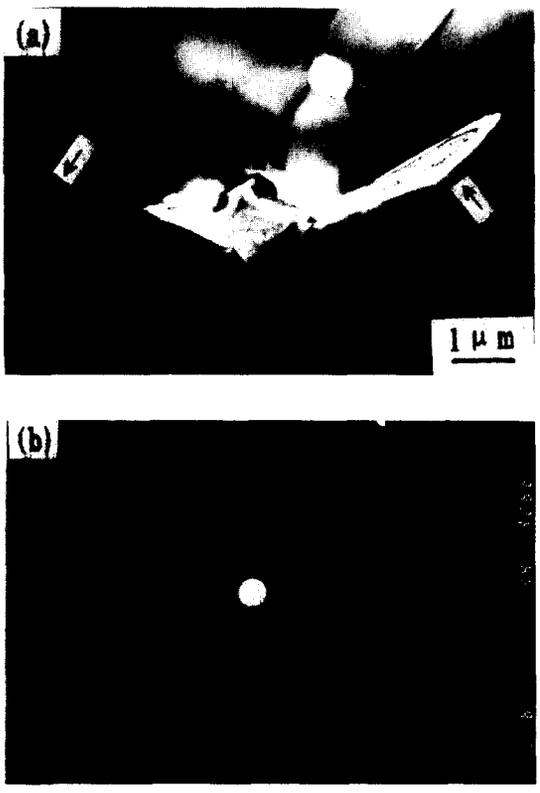

Fig. 3. Transmission electron micrographs of the crystal grain boundary phases. (a) Bright field image, (b) SADP. The arrows indicate the grain boundary phases.

cluded to be a kind of Al-rich compound with a chemical formula

$$(Al_2O_3)_x(Y_2O_3)_y(ZrO_2)_z(x + y + z = 1).$$

The amount of the crystal grain boundary phases is quite large; they are distributed at grain boundaries and Al_2O_3/ZrO_2 interfaces.

Another type of grain boundary phase is shown is Fig. 4. This type of grain boundary phase is rarely found in the specimens, they are distributed at triple points (Fig. 4(a)) and Al_2O_3/ZrO_2 interfaces (Fig. 4(b)). The SADP of the grain boundary phases (Fig. 4(c)) indicates that they are amorphous, and corresponding EDAX measurement (Table 5) discovers impurities Si and Ca, besides the enrichment of Al. The grain boundaries without amorphous phases are quite clean, no impurities such as Si and Ca are presented there.

According to these analyses, it can be concluded that there are three forms of Al_2O_3 in existence in ZrO_2. They are: (1) a very small amount of Al_2O_3 is dissolved in ZrO_2 grains; (2) the surplus Al_2O_3 then forms Al_2O_3 particles, which are extensively situated intra- and intergranularly; (3) Al_2O_3 segregates at grain boundaries, and forms the crystal and the amorphous Al-rich grain boundary phases; the amorphous one contains impurities such as Si and Ca.

Table 5. Composition of the amorphous grain boundary phases measured by EDAX

Element	*wt%*	*Oxide%*
Al	9·26	17·50
Si	29·40	62·91
Ca	8·00	11·20
Y	4·43	5·63
Zr	2·48	3·35

Fig. 4. Transmission electron micrographs of the amorphous grain boundary phases. (a), (b) Bright field images, (c) SADP. The arrows indicate the grain boundary phases.

4 Discussions

4.1 Effect of Al_2O_3 on the grain boundary resistance of ZrO_2

Al_2O_3 can reduce the ZrO_2 grain boundary resistance. Butler & Drennan suggested that this is because that Al_2O_3 acts as a scavenger for SiO_2 located at grain boundaries.[13] There are two types of grain boundary phases in ZrO_2, the crystal and the amorphous. Table 2 shows that the ZrO_2 grain boundary resistance is controlled by the Al_2O_3 addition and that Al_2O_3 reduces the R_{gbs}. This phenomenon may be explained with two mechanisms that are related to the two types of grain boundary phases.

Mechanism I: the Al_2O_3 addition scavenges SiO_2 located at grain boundaries and results in a low grain boundary resistance. This is similar to the results of Butler & Drennan. The only difference from the experiment of Butler & Drennan is that the specimens used in this paper contain CaO as well as SiO_2. According to the $CaO–Al_2O_3–SiO_2$ phase diagram,[14] CaO, Al_2O_3 and SiO_2 with a concentration relation listed in Table 5 will react with each other according to the following equation:

$$CaO + Al_2O_3 + 2SiO_2 \rightarrow CaAl_2Si_2O_3 \quad (5)$$

The impurities CaO and SiO_2 are transported by grain boundary diffusion to the triple points with high Al_2O_3 concentration and the Al_2O_3 particle surface, and by the chemical reaction (5), the grain boundary impurities are scavenged, and as a result, E_{gb} decreases.

Mechanism II: The crystal grain boundary phases contain no CaO or SiO_2, so the mechanism I can not explain all the experimental phenomena. And besides, the positron annihilation results show that Al_2O_3 increases the crystal defect concentration in ZrO_2. The defects can be roughly divided into two main parts, the defects in grains and those in the crystal grain boundary phases. The defects in grains are determined by the dopant Y_2O_3, and the Al_2O_3 solubility in grains is very low, so the effect of Al_2O_3 on the grain defects is negligible. This means that the increased crystal defect concentration is a result of the increasing of crystal defects in the crystal grain boundary phases, and consequently the resistance of the crystal grain boundary phases is very low, so the R_{gbs} subsequently decreases. Thus a new mechanism is derived as follows: the Al_2O_3 segregated at grain boundaries forms crystal grain boundary phases with very high defect concentration, so the grain boundary resistance decreases. Aono and coworkers observed a somewhat similar phenomenon in the solid electrolyte based on $LiTi_2(PO_4)_3$[15,16] in which grain boundary conductivity increases considerably by adding Li_3BO_3 or $Li_4P_2O_7$. The reason for the conductivity enhancement was attributed to the enhancement of the lithium concentration at the grain boundaries and the formation of a new conductive phase at the grain boundaries.

It should be noted that the enhancement of the ionic conductivity of some compounds by the incorporation of fine non-conduction particles seems to be quite popular,[17,18] It was usually considered to be due to the formation of conductive, defect-rich interfaces. This explanation is not quite applicable to the phenomena observed in this study, because Fig. 1(d) shows that the intragranular Al_2O_3 particles are accompanied by pores, and no such defect-rich interfaces were found for them, only for the intergranular Al_2O_3 particles, where such defect-rich interfaces were observed. So it must be stressed that the inter- and intragranular particles have different effects on the conductivity, when there are large difference in properties between the particles and the matrix, the conductive, defect-rich interfaces can only form for the intergranular particles.

4.2 Effect of grain boundaries on the emf of the ZrO_2 oxygen sensor

As an oxygen ion conductor, ZrO_2 is popularly used in oxygen sensors. By the emf output of the oxygen sensor, the oxygen partial pressure in all kinds of atmospheres can be measured. There are lots of factors affecting the emf output, the principle ones are electrode structure, electrode/electrolyte interfaces and ZrO_2 microstructure. In a practical process of an oxygen sensor, all the above factors simultaneously bring about an influence, and it is almost impossible to differentiate the individual influences by experiments, therefore, the effect of the grain boundaries on the output of the ZrO_2 oxygen sensors is analysed with a simplified model as follows.

Figure 5 is a simplified schematic representation of an oxygen sensor containing grain boundary phases. Suppose $t_i<1$ for the grain boundary phases, because the current through the grain boundary phases is also carried by oxygen ions; apart from an increase of internal resistance, the grain boundary phases do not influence the exclusively ionic nature of the conductivity of ZrO_2. The emf of the oxygen sensor can be given by eqn (6),[19] if the

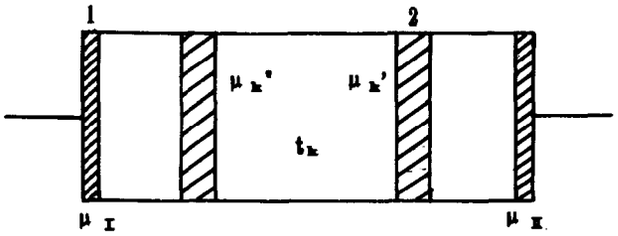

Fig. 5. Simplified schematic representation of an oxygen sensor. 1, Electrode; 2, grain boundary phases.

oxygen sensor is divided into several parts, as shown in Fig. 5. The meaning of t_k, μ_k'' and μ_k' can be seen from Fig. 5.

$$E = -\frac{1}{2ZF}\int_{\mu_I}^{\mu_{II}} t\,\mathrm{d}\mu$$

$$= -\frac{1}{2ZF}\sum t_k(\mu_k'' - \mu_k') \qquad (6)$$

When $t_k = 1$, the chemical potential of the region k can be totally transferred into the emf; when $t_k < 1$ and $\mu_k'' - \mu_k' = 0$, or $t_k = 0$ and $\mu_k'' - \mu_k' \neq 0$, the region k does not make any contribution to the emf. Under this condition, $E = E_{th}$ is held true, E_{th} being the theoretical value. When $t_k < 1$ and $\mu_k'' - \mu_k' \neq 0$, then $E < E_{th}$. When oxygen partial pressures over the electrodes are changed, during a transient situation, an appreciable oxygen potential drop may occur over the grain boundary phases, if $t_k < 1$ this yields a deviation from the E_{th} and an emf drift. Because the chemical diffusion inside ZrO_2 is very slow, the emf drift will last as long as several hours.

There are three kinds of grain boundary regions in the ZrO_2 with Al_2O_3 addition, the 'clean' grain boundaries but with Al segregation, the grain boundaries with amorphous phases and the grain boundaries with crystal phases. As Kingery has pointed out,[20] the ionic nature of ceramic oxide always leads to the formation of an electrostatic potential on grain boundaries, the sign and magnitude of the electrostatic potential depending strongly on impurity concentration. The Al segregation at the 'clean' grain boundaries certainly will change the grain boundary electrostatic potential, so the μ_k', μ_k'' values are changed, but although the nature of the 'clean' grain boundaries is unclear, $t_i = 1$ will hold true from them, thus the 'clean' grain boundaries do not have a negative effect on the emf. For the amorphous grain boundary phase, supposing $t_i = 0$ may be reasonable, and the amount of the amorphous phases is very limited, then according to this discussion the amorphous phases make no contribution to the emf. This means that the amorphous phases also do not have a negative effect on the emf. As proved by the present experiments, the crystal grain boundary phases are very conductive, and it can be seen from the Nernst–Einstein equation

$$D = \frac{\sigma KT}{CZ^2} \qquad (7)$$

where D is the charge carrier's diffusivity, C is the concentration of charge carrier, Z the charge quantity, and K and T have their usual meanings, that the oxygen ion diffusivity in the crystal grain boundary phases is very high. As long as chemical diffusivity in the grain boundary phases is very high, there will be practically no oxygen concentration drop (that is, chemical potential drop) over these phases. Therefore, for the crystal grain boundary phases $\mu_k'' - \mu_k' = 0$ might hold true, and then the phases will also possibly not have a negative effect on the emf of the oxygen sensor, notwithstanding that $t_i = 1$ or $t_i < 1$ for the crystal grain boundary phases. As the Al_2O_3 addition can scavenge the grain boundary impurities, it can be concluded that the Al_2O_3 segregation at the grain boundaries not only does not have a negative effect on the emf of the ZrO_2 oxygen sensor but also can release, even wipe out the detrimental effects of the other impurities, e.g. SiO_2.

5 Conclusion

The Al_2O_3 addition up to 5 mol% can reduce the grain boundary resistance per unit surface area of the grain boundaries and the activation energy for the grain boundary resistance of the 9 mol% Y_2O_3-stabilized ZrO_2. This is due to the scavenging of the impurities segregated at the grain boundaries, e.g. SiO_2, by Al_2O_3 and the formation of the Al-rich crystal grain boundary phases with very high defect concentration. The Al_2O_3 addition has no detrimental effect on the emf of the ZrO_2 oxygen sensor. All of this proves that the Al_2O_3-containing Y_2O_3-stabilised ZrO_2 is a kind of very good solid electrolyte and that to decrease the grain boundary resistance by adding new ingredients is a feasible way to further enhance the ionic conduction of ZrO_2. The next step that should be taken is to explore more oxides with characteristics similar to Al_2O_3.

References

1. Yen, T. S., The microstructure and properties of ceramics. 1. The development of ceramic microstructure and modern methods of investigation. *J. Chin. Ceram. Soc.*, **9** (1981) 64–79.
2. Badwal, S. P. S. & Drennan, J., Yttria–zirconia: effect of microstructure on conductivity. *J. Mat. Sci.*, **22** (1987) 3231–9.
3. Etsell, T. H. & Flengas, S. N., The electrical properties of solid oxide electrolyte. *Chem. Rev.*, **70** (1970) 339–76.
4. Badwal, S. P. S & Hughes, A. E., The effects of sintering

atmosphere on impurity phase formation and grain boundary resistivity in Y_2O_3-fully stabilized ZrO_2. *J. Eur. Ceram. Soc.*, **10** (1992) 115–22.
5. Keiger, K., Burggraaf, A. J. & De With, G., The effect of Bi_2O_3 on the electrical and mechanical properties of ZrO_2–Y_2O_3 ceramics. *J. Mat. Sci.*, **17** (1982) 1095–102.
6. Verkerk, M. J., Winnubst, A. J. A. & Burggraaf, A. J., Effect of impurities on sintering and conductivity of yttria-stabilized zirconia. *J. Mat. Sci.*, **17** (1982) 3113–22.
7. Radford, K. C. & Bratton, R. J., Zirconia electrolyte cells. Part 1. Sintering studies. *J. Mat. Sci.*, **14** (1979) 59–65.
8. Miyayama, M., Yanagida, H. & Asada, A., Effects of Al_2O_3 additions on resistivity and microstructure of yttria-stabilized zirconia. *Am Ceram. Soc. Bull.*, **65** (1985) 660–4.
9. Bauerle, J. E., Study of solid electrolyte polarization by a complex admittance method. *J. Phys. Chem. Solids*, **30** (1969) 2657–70.
10. Miyayama, M. & Yanagida, H., Dependence of grain-boundary resistivity on grain-boundary density in yttria-stabilized zirconia. *J. Am. Ceram. Soc.*, **67** (1984) C194–5.
11. Brandt, W. & Dupasquier, A., *Positron Solid State Physics*. North Holland, Amsterdam, 1983, p. 24, p. 200.
12. Bernard, H., Sintered stabilized zirconia microstructure and conductivity. Report CEA-R-5090, Commissariat à l'Energie Atomique, CEN-Saclay, France, 1981, p. 117.
13. Butler, E. P. & Drennan, J., Microstructural analysis of sintered high-conductivity zirconia with Al_2O_3 additions. *J. Am. Ceram. Soc.*, **65** (1982) 474–8.
14. Gottwald, G., Forkel, K. & Wihsmann, F. G., Computer assisted design of phase diagrams. *Silikattechnik*, **36** (1985) 49–53.
15. Aono, H. & Sugimoto, E., Ionic conductivity of solid electrolytes based on lithium titanium phosphate. *J. Electrochem. Soc.*, **137** (1990) 1023–7.
16. Aono, H., Sugimoto, E., Sadaoka, Y., Imanaka, N. & Adachi, G., Ionic conductivity of $LiTi_2(PO_4)_3$ mixed with lithium salts. *Chem. Lett.*, **219** (1991) 331–4.
17. Liang, C. C., Conduction characteristics of the lithium iodide-aluminum oxide solid electrolytes. *J. Electrochem. Soc.*, **120** (1973) 1289–92.
18. Jow, T. & Wagner, Jr, J. B., The effect of dispersed alumina particles on the electrical conductivity of cuprous chloride. *J. Electrochem. Soc.*, **126** (1979) 1963–72.
19. Beekmans, N. M & Heyne, L., Correlation between impedance microstructure and composition of calcia-stabilized zirconia. *Electrochem. Acta*, **12** (1976) 303–10.
20. Kingery, W. D., Plausible concepts necessary and sufficient for interpretation of ceramic grain-boundary phenomena: 1. Grain-boundary characteristics, structure, and electrostatic potential. *J. Am. Ceram. Soc.*, **57** (1974) 1–8.